Elsevier Editorial System(tm) for ISPRS Journal of Photogrammetry and Remote Sensing
Manuscript Draft

Manuscript Number: PHOTO-D-20-00051R2

Title: A marker-free method for registering multi-scan terrestrial laser scanning data in forest environments

Article Type: Research Paper

Section/Category: Laser scanning

Keywords: Terrestrial laser scanning; registration; marker free; forest

Corresponding Author: Dr. Yanjun Su, Ph.D.

Corresponding Author's Institution: Institute of Botany, Chinese Academy of Sciences

First Author: Hongcan Guan

Order of Authors: Hongcan Guan; Yanjun Su, Ph.D.; Xiliang Sun; Guangcai Xu, Ph.D.; Wenkai Li, Ph.D.; Qin Ma; Xiaoyong Wu; Jin Wu, Ph.D.; Lingli Liu, Ph.D.; Qinghua Guo, Ph.D.

# A marker-free method for registering multi-scan terrestrial laser scanning data in forest environments

Hongcan Guan[1,2], Yanjun Su[1,2], Xiliang Sun[1,2], Guangcai Xu[1,2], Wenkai Li[3], Qin Ma[1,2], Xiaoyong Wu[1,2], Jin Wu[4], Lingli Liu[1,2], Qinghua Guo[1,2]

[1]State Key Laboratory of Vegetation and Environmental Change, Institute of Botany, Chinese Academy of Sciences, Beijing 100093, China

[2]University of Chinese Academy of Sciences, Beijing 100049, China

[3]School of Geography and Planning, Sun Yat-Sen University, Guangzhou 510275, China

[4]School of Biological Sciences, University of Hong Kong, Pokfulam, Hong Kong

# Highlights

- A novel marker-free multi-scan TLS registration method is proposed.
- It uses the occlusion effect of tree trunks in TLS scans as the key features.
- It does not require processing steps to extract individual tree attributes.
- The proposed method is tested in plots with different vegetation conditions.
- Its registration accuracy is equivalent to the manual registration method.

# A marker-free method for registering multi-scan terrestrial laser scanning data in forest environments

## Abstract

Terrestrial laser scanning (TLS) has been recognized as an accurate means for non-destructively deriving three-dimensional (3D) forest structural attributes. These attributes include but are not limited to tree height, diameter at breast height, and leaf area density. As such, TLS has become an increasingly important technique in forest inventory practices and forest ecosystem studies. Multiple TLS scans collected at different locations are often involved for a comprehensive characterization of 3D canopy structure of a forest stand. Among which, multi-scan registration is a critical prerequisite. Currently, multi-scan TLS registration in forests is mainly based on a very time-consuming and tedious process of setting up hand-crafted registration targets in the field and manually identifying the common targets between scans from the collected data. In this study, a novel marker-free method that automatically registers multi-scan TLS data is presented. The main principle underlying our method is to identify shaded areas from the raw point cloud of a single TLS scan and to use them as the key features to register multi-scan TLS data. The proposed method is tested with 17 pairs of TLS scans collected in six plots across China with various vegetation characteristics (e.g., vegetation type, height, understory complexity). Our results showed that the proposed method successfully registered all 17 pairs of TLS scans with equivalent accuracy to the manual registration approach. Moreover, the proposed method eliminates the process of setting up registration targets in the field, manually identifying

registration targets from the TLS data, and processing the raw TLS data to extract individual tree attributes, which brings it the advantages of high efficiency and robustness. It is anticipated that the proposed algorithms can save time and cost of collecting TLS data in forests, and therefore improves the efficiency of TLS forestry applications.

***Keywords*****:** Terrestrial laser scanning; registration; marker-free; forest

## 1. Introduction

Terrestrial laser scanning (TLS) technique has been recognized as an important and accurate method for forest inventory and ecosystem studies (Dassot et al., 2011; Bauwens et al., 2016; Liang et al., 2016). Through emitting dense laser pulses, it can be used to acquire three-dimensional information of standing trees in millimeter-level accuracy (Cabo et al., 2018), and therefore retrieve traditional forest structural parameters (e.g. tree height, diameter at breast height/DBH, canopy cover, leaf area index) and beyond (e.g., leaf area density, branching architecture) (Olsoy et al., 2016; Li et al., 2017; Zhu et al., 2017). Due to the occlusion effect (by tree stems, branches, and leaves), the “stop-and-go” mode is commonly used to scan a forest stand so that a complete TLS point cloud can be obtained from multiple scans (Lin et al., 2012; Panagiotidis et al., 2016). As a consequence, multi-scan TLS data registration has become a critical pre-requisite for TLS forestry applications (Hilker et al., 2012).

Exterior features (e.g., navigation information from Global Navigation Satellite System/GNSS and inertial measurement unit/IMU, geometric information from the environment) are usually needed to register point clouds collected from different scanning locations. Due to the fact that the GNSS signal can be easily blocked or influenced by multipath effect under forest canopy (Sigrist et al., 1999), using navigation information from GNSS and IMU to directly register multi-scan TLS data is not accurate. Recent developments in the simultaneous localization and mapping algorithm bring new opportunities in automatically registering TLS point clouds from navigation information, however its accuracy is much lower than single-scan TLS data (Lin et al., 2014). Moreover, the complexity and irregularity of forest environments may give rise to the absence of repeatable and unambiguous features in TLS data, which are required by registration methods based on geometric features (Theiler et al., 2015; Guan et al., 2019). To solve this issue, one of the most commonly used methods is to manually set up hand-crafted registering targets in the scanning environment and register TLS scans by manually identifying and matching these targets from TLS point clouds. Although the manual registration approach can achieve high registration accuracy (Hilker et al., 2012; Liang et al., 2018), it is very time-consuming to set up registration targets in the field, and manually identifying and matching registration targets from TLS point clouds could be difficult in forests due to the occlusion of branches and leaves (Wang et al., 2008; Basantes et al., 2019). A major bottleneck for the application of TLS in large-scale forest managements and studies is how to automatically register multi-scan TLS data with high accuracy.

Recently, numerous efforts have been put forth in developing marker-free methods to register multi-scan TLS data in forest environments. These methods typically used individual tree attributes (e.g., tree location, tree height, DBH) as the required exterior features for registration. For example, Henning and Radtke (2008) identified tree stem centers as tie points and used them in an ICP registration procedure; Liu et al. (2017) reconstructed stem curves from each TLS scan and then matched tree stems between scans at the feature level to achieve the goal of registering multi-scan TLS data; Kelbe et al. (2016) and Tremblay and Béland (2018) used tree locations and DBHs derived from tree stem maps as the features to perform multi-scan TLS registration. Moreover, certain multi-platform point cloud registration methods also showed great potential in registering multi-scan TLS data. For example, Guan et al. (2019) proposed an automatic multi-platform point cloud data registration framework based on tree locations, which has shown the success in registering multi-scan TLS data in coniferous forests; Polewski et al. (2019) proposed a method to register multi-platform point cloud data in forested areas through constructing a similarity distance measure of tree stems. However, promising the abovementioned marker-free methods are, they all require specific individual tree attributes (e.g., tree location, tree height, DBH, stem maps) obtained through a series of post-processing steps (e.g., ground point filtering, normalization, individual tree segmentation). The post-processing steps of raw TLS data can be very time consuming, involving very tedious manual editing and correction in complex forest environments, to obtain accurate enough tree attributes (Brolly and Király, 2009; Trochta et al., 2013; Heinzel and Huber, 2017).

This study presents a marker-free algorithm for accurately registering multi-scan TLS data in forested areas without the need of processing raw TLS data to extract individual tree attributes.

The main principle of the proposed algorithm is to identify and use shaded areas in TLS point clouds as the key feature to match adjacent TLS scans. The developed algorithm was tested in six study plots with different vegetation types (i.e., planted coniferous forest, natural mixed conifer and broadleaf forest, and rainforest) across China. We believe the proposed algorithm can greatly improve the TLS data registration efficiency since it is an automatic method purely based on raw TLS data, and has great potential to be used in large-scale TLS data collection for forest managements and studies.

## 2. Data and Methodology

### 2.1 Study area

Six study plots were selected across China, including one planted temperate coniferous forest plot (plot 1), three temperate mixed conifer and broadleaf forest plots (plots 2-4) and two rainforest plots (plots 5 and 6) (Figure 1a). Plot 1 is located in Mulan Paddock (Hebei Province) with an area of 45 m × 45 m (Figure 1c), and the dominant tree species are *Pinus tabuliformis Carrière* and *Pinus sylvestris var. mongolica Litv* with few understory shrubs (Table 1 and Figure 1b). Trees here are planted regularly with similar age and height. The average tree height is 17 m, the canopy cover is 71%, and the tree density is 1056 trees/ha (Table 1). Plots 2-4 are located in Yichun (Heilongjiang Province), Dongling Mountain (Beijing) and Changbai Mountain (Jilin Province) with an area ranging from 30 m × 30 m to 35 m × 35 m (Figure 1c). Trees in these three plots are mixed with conifers (e.g., *Pinus koraiensis* and *Pinus tabuliformis Carrière*) and broadleaves (e.g., *Quercus mongolica*, *Populus ussuriensis*, and *Betula platyphylla*) (Table 1). The average tree height of plots 2-4 is 19 m, 13 m, and 18 m, and the canopy cover is 92%, 93% and 84% (Table 1), respectively. The tree density increases from plot 1 to plot 3, and the understory shrubs become more complex than plot 1 (Figure 1b). Plots 5 and 6 are rainforest located in Jianfengling (Hainan Province) with an area of 30 m × 30 m (Figure 1c). The dominant tree species are *Microcos paniculata* and *Terminalia nigrovemulosa*, the average tree height is around 16 m, and the average canopy cover is around 90% (Table 1). The tree density in these two plots is the highest among all plots (>2000 trees/ha), and the undercanoy vegetation is dominated by lianas (Figure 1b).

**Table 1** Tree attribute summary of the six study plots.

| ID | Forest type | Dominant tree species | Tree height (m) | Canopy cover (%) | Tree density (trees/ha) |
|---|---|---|---|---|---|
| 1 | Planted temperate coniferous forest | *Pt, Ps* | 17 | 71 | 1056 |
| 2 | Temperate mixed conifer and broadleaf forests | *Pk, B.* | 19 | 92 | 912 |
| 3 | Temperate mixed conifer and broadleaf forests | *Pt, Q.* | 13 | 93 | 1009 |
| 4 | Temperate mixed conifer and broadleaf forests | *Pk, Pu* | 18 | 84 | 1023 |
| 5 | Rainforest | *M., T.* | 16 | 89 | 2365 |
| 6 | Rainforest | *M., T.* | 17 | 91 | 2147 |

Note that *Pt* represents *Pinus tabuliformis Carrière*; *Ps* represents *Pinus sylvestris var. mongolica Litv*; *Pk* represents *Pinus koraiensis*; *B* represents the *Betula platyphylla*; *Q.* represents *Quercus mongolica*; *Pu* represents the *Populus ussuriensis*; *M.* represents *Microcos paniculata*; and *T.* represents *Terminalia nigrovemulosa.*

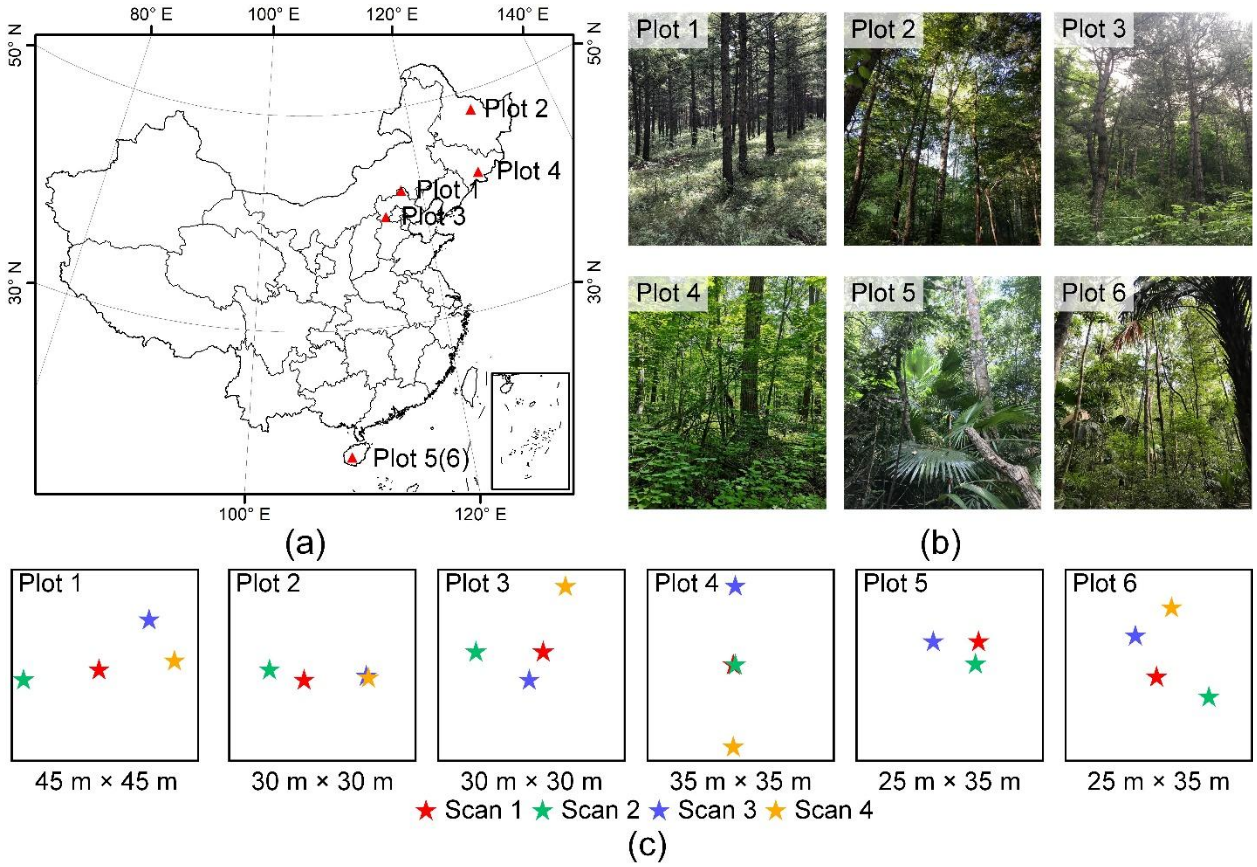


**Figure 1** (a) The location of the six selected study plots; (b) photo examples of each study plot; (c) illustration of the TLS scan setup in each study plot.

## 2.2 TLS data collection

A RIEGL VZ-400 scanner mounted on a tripod was used to collect TLS data within each plot. It is a high-precision TLS scanner with a specified ranging accuracy of ±5 mm. Its maximum measurement range is from 350 m (high-speed mode) to 600 m (long-range mode), and its minimum measurement range is 1.5 m. The RIEGL VZ-400 scanner can provide a maximum field of view of 360° horizontally and 100° vertically (from -40° to 60°). Within each plot, at least three TLS scans were collected using the setup shown in Figure 1c. The average distance between scan centers was 9.9 m, and the maximum distance was 21.6 m. At least five high-reflectance referencing targets were installed in each plot for manual registration. All scans were set up horizontally (i.e., perpendicular to the ground), with the exception of scan 4 in plot 2 and scan 2 in plot 4. These two scans were set up with a tilting angle of 30° approximately to get complete vertical information of forest canopy, which is a commonly used TLS scanning strategy in forests with dense and tall canopies (Wilkes et al., 2017; Roşca et al., 2018).

### 2.3 Overview of the proposed marker-free TLS registration method

The main principle of the proposed marker-free TLS registration is to use shaded areas from tree trunks, branches and leaves as the key feature to register multi-scan TLS data. As shown in Figure 2, laser pulses cannot penetrate tree trunks and would leave a shaded area behind it. The starting point of a shaded area (in the ray direction from the scan center) can be treated as a potential tree location. Adjacent TLS scans should share common trees in overlapped areas, and the identified tree locations through shaded areas could be used as the features to register multi-scan TLS data (Figure 2b). Therefore, the proposed marker-free TLS registration method hinges upon the successful extraction of the starting points of shaded areas from each TLS scan, which is defined as visual occlusion points hereafter.

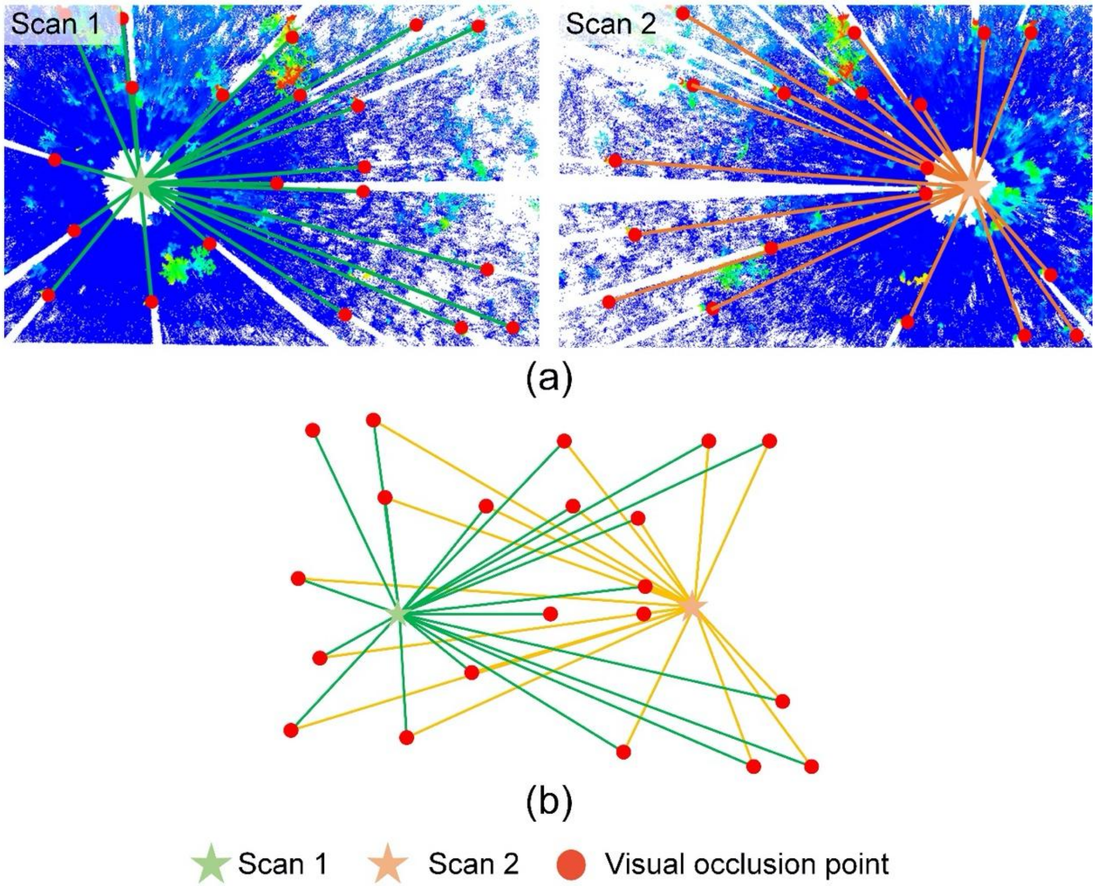


**Figure 2** Schematic diagram of the proposed marker-free registration method. (a) represents the occlusion effect of tree trunks in a single TLS scan and (b) indicates the spatial relationship between the visual occlusion points from two neighboring TLS scans.

The workflow of the proposed algorithm can be divided into three steps, which are data redundancy reduction, coarse registration and fine registration (Figure 3). The data redundancy reduction step aims to increase the registration speed by reducing unnecessary data. The coarse registration is the key step of the proposed algorithm, which can be further divided into vertical coarse registration, visual occlusion point extraction and horizontal coarse registration (Figure 3). Vertical coarse registration aims to translate a TLS target scan in the *Z* direction so that it can be coarsely matched with the corresponding TLS source scan vertically. Visual occlusion point extraction uses a segmentation strategy based on an angular grid generated from a TLS scan. Finally, the horizontal coarse registration aims to find the shared visual occlusion points through an enumeration procedure and calculate the horizontal rotation and translation matrices. After the coarse registration step, the fine registration step uses the ICP the algorithm to further improve the registration accuracy and generate the registered point cloud. Detailed information of each step is presented in the following sections.

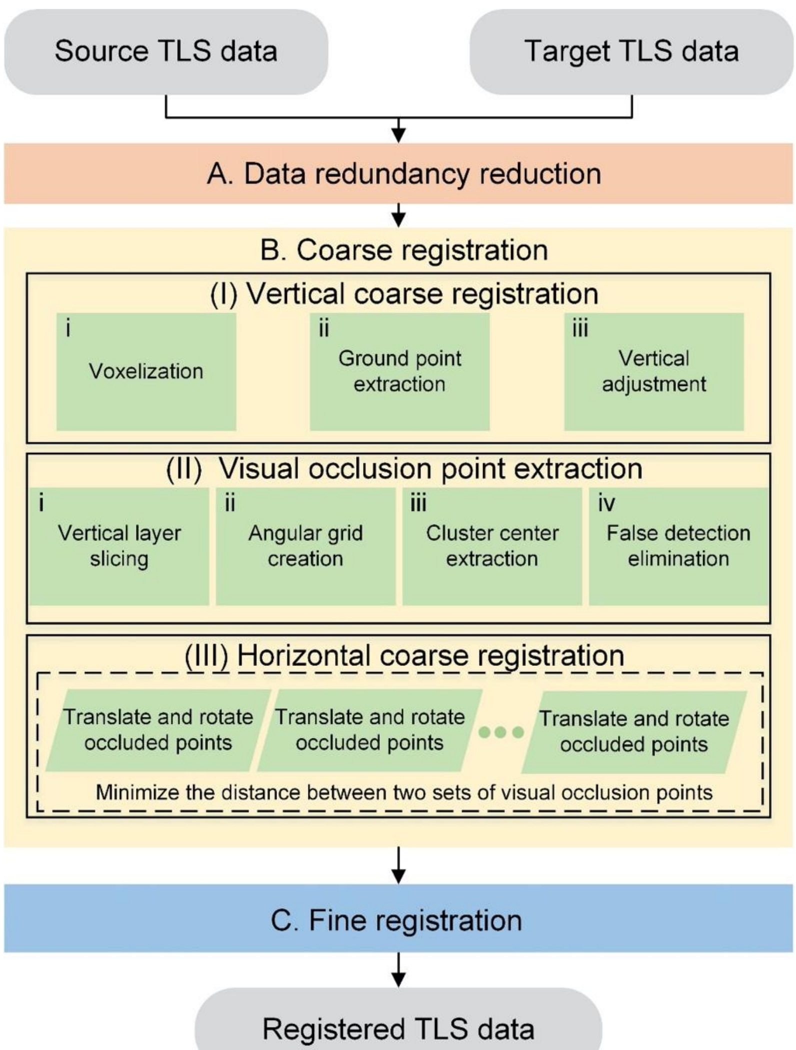


**Figure 3** Workflow of the proposed algorithm for registering multi-scan TLS data in forests.

## 2.4 Data redundancy reduction

TLS scanners typically have a long-range detection capability of more than hundreds of meters, and the point density usually decreases significantly with the increase of the distance to the scanner (Figure 2a). Points far away from the scanner are less useful for the registration than points close to the scanner due to the limited overlaps between the source and target TLS scans. However, if we include all points in the registration process, it can significantly slow down the registration speed. Therefore, the proposed algorithm first excludes points that are far away from the scanner through the use of a defined horizontal distance threshold $D_c$. For a laser point $i$, its horizontal distance to the scanner center $D$ can be calculated as,

$$D = \sqrt{(x_i - x_s)^2 + (y_i - y_s)^2} \quad (1)$$

where $(x_i, y_i)$ is the horizontal coordinates of the laser point $i$ in its local coordinate system, which is referred to as the Scanner's Own Coordinate System (SOCS) hereafter, and $(x_s, y_s)$ is the horizontal coordinates of the laser scanner in SOCS. If $D$ is larger than the predefined threshold $D_c$, the corresponding point should be excluded. The following coarse registration step is based on the reduced TLS data.

## 2.5 Coarse registration

### *2.5.1 Vertical coarse registration*

Previous studies have proven that the ICP algorithm is a robust method to align two point cloud data into a similar height (Henning and Radtke, 2006; Travelletti et al., 2013), which usually requires accurate ground points as inputs. However, extracting accurate ground points from raw TLS data needs the assistance of complex ground point filtering algorithms, which is a time-consuming step (Pirotti et al., 2013; Che and Olsen, 2017). The incomplete point cloud from a single TLS scan may bring problematic filtering results since filtering algorithms are highly influenced by the point density (Zhao et al., 2018). To accelerate and simplify this process, the proposed method uses a voxel-based procedure to identify ground points (Figure 4). Input TLS data is first voxelized and then the corresponding voxel index ($G_x, G_y, G_z$) of a point ($x$, $y$, $z$) is calculated using the following equation,

$$\begin{cases} G_x = int(\frac{x - x_{min}}{voxel\ size}) \\ G_y = int(\frac{y - y_{min}}{voxel\ size}) \\ G_z = int(\frac{z - z_{min}}{voxel\ size}) \end{cases} \quad (2)$$

where *int* represents the operation of rounding a number to its nearest integer; $x_{min}$, $y_{min}$, and $z_{min}$ are the minimum *x*, *y*, and *z* coordinates of all points in the TLS data. TLS points with the minimum $G_z$ in each combination of $G_x$ and $G_y$ are labeled as ground points, while others are labeled as vegetation points. After the ground point extraction, the identified ground points from the source and target TLS data are then used to run the ICP algorithm for calculating the vertical transformation matrix for vertical coarse registration. Note that the identified ground points here may include noise points of low vegetation. Nevertheless, they should not have a significant influence on the vertical coarse registration results since the ICP-based vertical matching procedure is insensitive to low-vegetation noise points (Henning and Radtke, 2006; Travelletti et al., 2013).

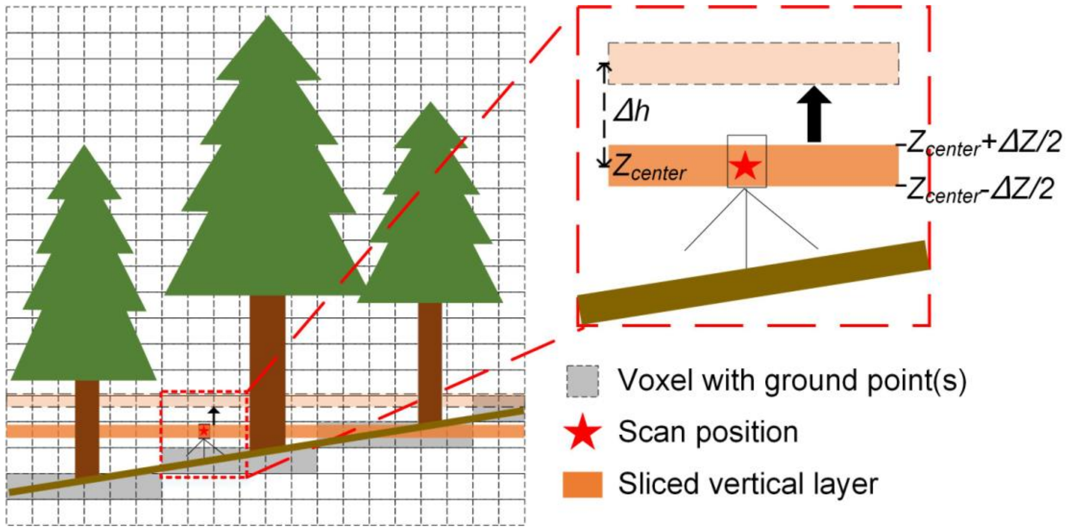


**Figure 4** An illustration of the voxelization and the vertical layer slicing. $Z_{center}$ represents the height of the scan center, $\Delta h$ represents the increased height from the scan center, and $\Delta Z$ represents the thickness of the sliced vertical layer.

*2.5.2 Visual occlusion point extraction*

Visual occlusion points are the key features of the proposed algorithm to register multi-scan TLS data. First, a vertical layer slicing procedure is used to extract potential tree trunk points since shaded areas are more easily observed in layers that include tree trunks. It should be noted that ground points identified from the previous step should be excluded in the visual occlusion point extraction step because they have very few contributions to detect shaded areas. The principle for determining the height of a sliced vertical layer is that it should contain as many tree trunk points as possible. The sliced vertical layer can be set at the height of the scanner (Figure 4) given that the TLS scanner is usually installed with the best visibility. Terrain effects should be considered during the slicing step by slicing multiple vertical layers (Figure 4) if the study area includes elevational changes. Visual examination can be used to determine how many layers should be sliced. The above slicing procedure can be described mathematically as,

$$Z_{HC} = Z_{center} + \Delta h \tag{3}$$

$$Z \in [Z_{HC} - \Delta Z/2, Z_{HC} + \Delta Z/2] \tag{4}$$

where *Z* represents the height of a point within the sliced vertical layer, $Z_{center}$ represents the height of the scan center, $\Delta h$ represents the increased height from the scan center, which could be zero in areas with flat terrain, and $\Delta Z$ represents the thickness of the sliced vertical layer. In order to eliminate the influence of a tilted scanner, it is recommended to use a horizontally placed scan as the source scan or applying a Z-axis adjustment to make the *Z*-axis be perpendicular to the ground (Polewski *et al.*, 2019).

After the vertical layer slicing procedure, a user-defined radius threshold $D_r$ ($D_r$<$D_c$) is used to further restrict the extent of the sliced layer(s) for extracting visual occlusion points. Within the extent of $D_r$, an angular grid is created with an angular resolution of $I_A$ and a distance resolution of $I_D$ (Figure 5a), which can be described as follows,

$$\begin{cases} i = int(\frac{A}{I_A}) \\ j = int(\frac{D}{I_D}) \end{cases} \tag{5}$$

where $(i, j)$ is the index of a pixel within the angular grid; *A* refers to the azimuth angle between a TLS point and the scan center, and $D$ refers to the horizontal distance from a TLS point to the scan center.

Each outermost pixel with vegetation points in every angular direction is a potential starting point of a shaded area and therefore is selected for further processing (Figure 5b). The connected component labeling (CCL) method is employed to further remove noise points (e.g., branch and leaf points). CCL is an algorithm based on graph theory that can label subsets of connected components based on a given heuristic (Miliaresis and Kokkas, 2007). Since tree trunks usually have a much higher point density than leaves, trunk points in remaining outermost pixels would likely be labeled as a connected component, while branch and leaf points would be labeled as separated components. The CCL algorithm in the CloudCompare software is integrated into the registration algorithm. It uses an octree structure to organize point cloud, which can greatly improve the computation efficiency. All points identified as connected components are kept for the detection of visual occlusion points, while others are excluded.

For the points of each identified connected component, the mean shift method is used to identify the center of a tree trunk. Trunk points of the same tree may have an offset from adjacent TLS scans due to the difference in TLS viewing angles, causing an error in registration results. To solve this issue, the location with the maximum local point density is assumed to be the center of a tree trunk. The mean shift method is a nonparametric segmentation method based on the assumption that the input set of points are sampled from the underlying probability distribution (Comaniciu and Meer, 2002) and it is an ideal approach for finding tree trunk centers because it iteratively moves the input data points to the densest point area until the center of mass converged (Ferraz et al., 2012; Hu et al., 2017). The mean shifted method is accelerated by only using the TLS points in a voxel with the most TLS points of a given component. As a result, the identified mass centers found by the mean shift algorithm are used as potential visual occlusion points.

The obtained potential visual occlusion points may still contain errors because dense branches or leaves might be misidentified as connected components by the CCL algorithm. A visibility examination step is further developed to improve the visual occlusion point identification accuracy. A rectangular buffer is created with the long side parallel to the radial direction from the scan center, and the starting point of the buffer has a distance of $D_e$ behind the corresponding visual occlusion point along the radial direction (Figure 5c). The width (short side) of the rectangular buffer is the same as the distance resolution of the angular grid $I_D$, and the long side of the buffer should be within $D_c$. If there were any TLS points within the rectangular buffer, the corresponding visual occlusion point is treated as a false detection and excluded from the horizontal coarse registration step.

Additionally, if the TLS scan was partitioned by multiple vertical layers (Figure 4), the visual occlusion points obtained at each vertical layer should be combined. If one or more visual occlusion points were found in each vertical layer with the same horizontal voxel index ($G_x$, $G_y$), only points at the bottom most layer are retained.

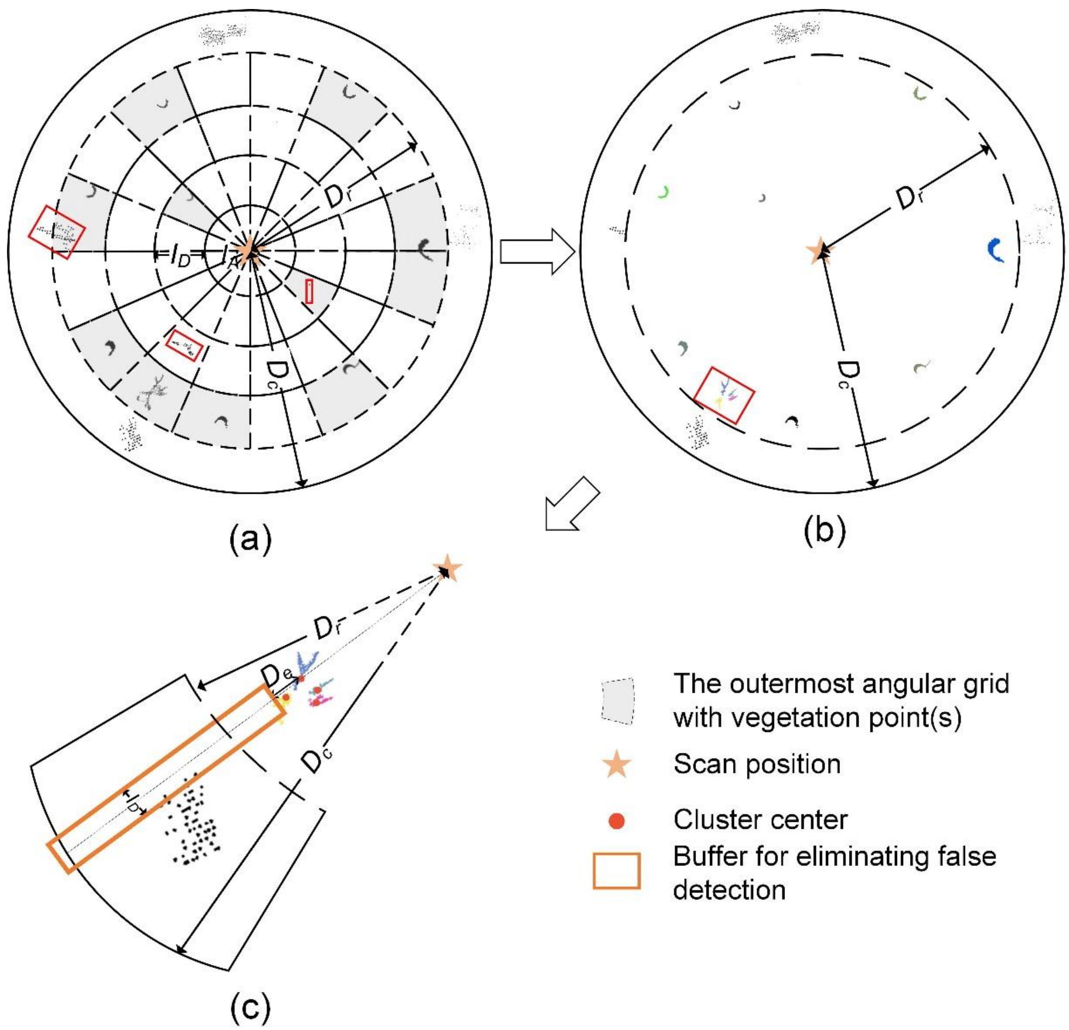


**Figure 5** (a) A schematic illustration for creating the angular grid of a TLS scan. The outermost angular grid with vegetation point(s) is marked with gray color and red boxes represent noise points (e.g., branch and leaf points). (b) The remained vegetation point(s) after the procedure of labeling connected components. (c) The creation of a buffer to determine whether a cluster center is a visual occlusion point.

*2.5.3 Horizontal coarse registration*

Using the above procedures, two sets of visual occlusion points can be extracted for the source TLS data and target TLS data, respectively. Using mathematical expressions, the visual occlusion points for the source and target TLS data can be written as $P_s = \{P_{s_1}, P_{s_2}, \dots, P_{s_m}\}$ and $P_t = \{P_{t_1}, P_{t_2}, \dots, P_{t_n}\}$, where *m* and *n* are the numbers of visual occlusion points in $P_s$ and $P_t$. To ascertain the horizontal relationship between $P_t$ and $P_s$, an enumeration process is used to match $P_t$ and $P_s$ by iteratively rotating and translating $P_t$, where the matching pair with the minimum overlapped distance is regarded as the solution for the horizontal coarse registration between $P_t$ and $P_s$ (Figure 6).

In order to solve the minimum overlapped distance between $P_t$ and $P_s$, a visual occlusion point $P_{t_{j,j\epsilon n}}$ in $P_t$ is first matched with the first point $P_{s_1}$ in $P_s$ (Figure 6a), and $P_t$ is translated to a new coordinate system $P_t'$ based on the horizontal distance between $P_{t_{j,j\epsilon n}}$ and $P_{s_1}$ (Figure 6b). Then, $P_t'$ is rotated counterclockwise iteratively with point $P'_{t_{j,j\in n}}$ as the rotation center, and the coordinate system is transformed to $P_t^{"}$ correspondingly (Figure 6c). The rotating angular interval is set as the same as the angular resolution of the angular grid $I_A$. The horizontal distance from each point in $P_t^{"}$ to its closest point in $P_s$, $d_{j\to i}$, is calculated for each rotation, and the overlapped distance of each rotation, $D_{overlap}$, is calculated as,

$$D_{overlap} = \sum_{j=1}^{n} \min\left(d_{j\to i}, D_t\right) \quad (6)$$

where $D_t$ is a pre-defined match distance threshold. Although the mean shift method is used to identify the center of tree trunks to reduce the influence of mismatches from different viewing angles, there still could be an offset existed in a visual occlusion point pair. If $d_{j\to i}$ is smaller than $D_t$, it is used for calculating $D_{overlap}$; otherwise, $D_t$ should be used to replace $d_{j\to i}$ to calculate $D_{overlap}$. The above translation and rotation processes are iterated by matching with every point in $P_s$, and all $D_{overlap}$ values are calculated. The rotation and translation matrices with the smallest $D_{overlap}$ are used as the optimum solution for matching source and target TLS scans, which can be described as follows,

$$(x,y)_{transformed} = R(arg\ min(D_{overlap})) \times (x,y)_{target} + T(arg\ min(D_{overlap})) \quad (7)$$

where $(x,y)_{target}$ is the horizontal coordinates of points in the target TLS scan, *arg min*$(D_{overlap})$ is the argument of the minimum $D_{overlap}$, *R* and *T* are the rotation and translation matrices from the solution with the minimum value of $D_{overlap}$, and $(x,y)_{transformed}$ is the transformed horizontal coordinates of points in the target TLS scan. The whole enumeration process can be described by the pseudo-code shown in Figure 7.

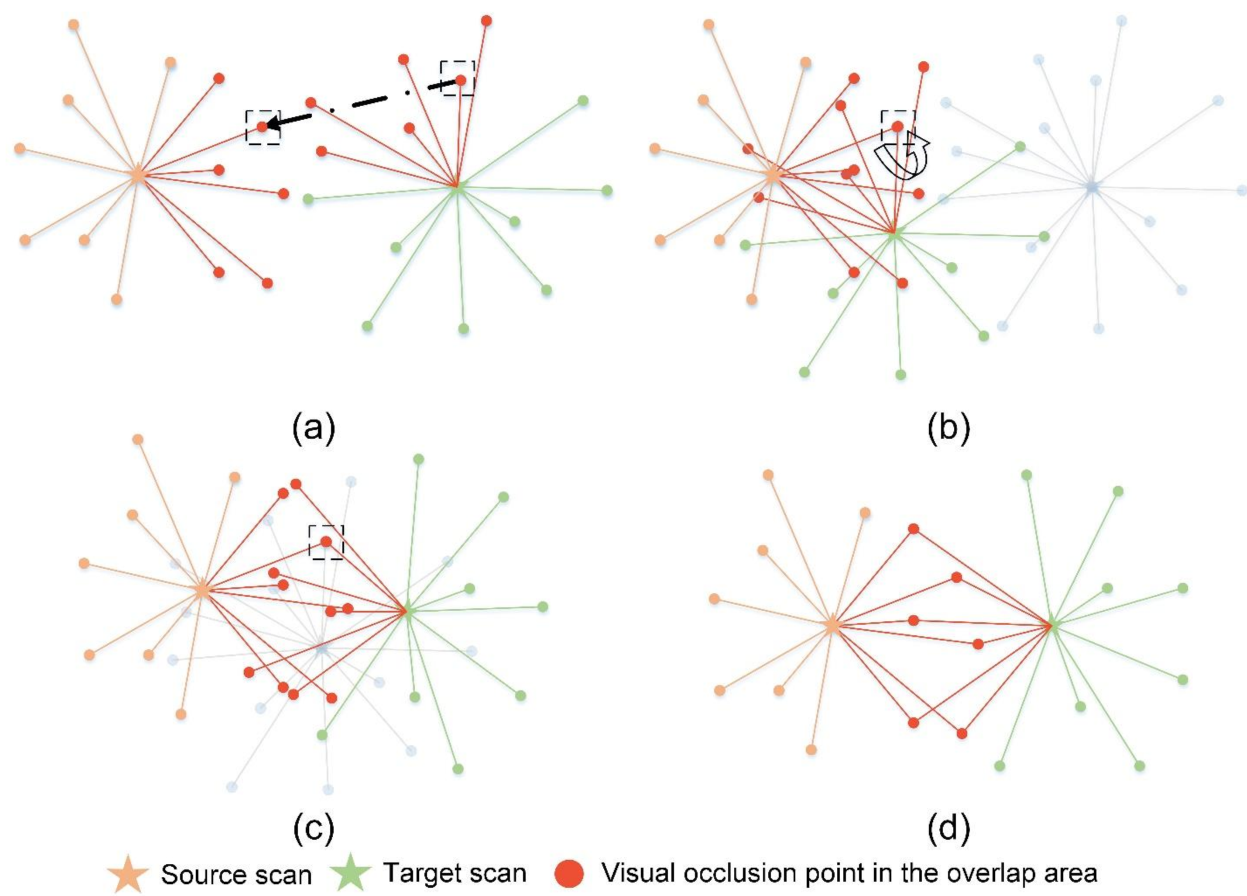

**Figure 6** (a) An illustration of the unordered visual occlusion points of the source scan ($P_s$) and target scan ($P_t$). The black dashed squares indicate a random point pair and the black dashed arrow indicates the translation based on the point pair. (b) An illustration of $P_s$ and $P_t$ after being horizontally translated. The curved arrow indicates the rotation direction. (c) An illustration of $P_s$ and $P_t$ after being horizontally rotated. (d) An illustration of the matched $P_s$ and $P_t$ solution with the minimum overlap distance.

---

Input data: Visual occlusion points $P_s$ of the source TLS scan and visual occlusion points $P_t$ of the target TLS scan

Output data: Rotation matrix *R* and translation matrix *T*

---

Function Enumeration $(P_s, P_t)$:

  For $P_{s_i} \epsilon P_s$ do

    For $P_{t_j} \epsilon P_t$ do

      Calculate horizontal translation between $P_{s_i}$ and $P_{t_j}$

      Move $P_t$ to $P_t^{'}$ according to the horizontal translation

      For $k = 1\ to\ 360/I_A$ do

        $\theta_{i,j,k} = k \times I_A$

        $D_{i,j,k} = 0$

        Rotate $P_t^{'}$ to $P_t^{''}$ according to $\theta_{i,j,k}$

        For $P_{s_i} \epsilon P_s$ *do*

          Calculate the minimum distance $d_{j \to i}$ between $P_{s_i}$ and $P_{t_j}^{''} \epsilon P_t^{''}$

          $D_{Overlap_{i,j,k}} = D_{Overlap_{i,j,k}} + min(d_{j \to i}, D_t)$

        End for

      End for

    End for

  End for

  Find minimum $D_{Overlap_{i,j,k}}$, and calculate *R* and *T* for the horizontal coarse registration

  Return *R* and *T*

---

**Figure 7** Pseudo-code for the enumeration process of finding the optimal transformation solution with the minimum overlapped distance for horizontal coarse registration.

## 2.6 Fine registration

The vertical and horizontal coarse registration provides initial estimates for the rotation and translations matrices for registering the source and target TLS scans. A fine registration step is needed to further improve the registration accuracy. The ICP algorithm is used here to minimize the cumulative distance between the source and target TLS data. Complete source and target TLS data are used as the inputs of the ICP algorithm. The ICP algorithm from the RIEGL RiScan Pro software was used to run the fine registration process in this study so that the registration results could be compared with manual registration results. Other open-source ICP modules (e.g., the ICP tool in CloudCompare software) can also be used for this step.

## 2.7 Experiment design and accuracy assessment

The developed marker-free multi-scan TLS registration algorithm was implemented with the C++ programming language in this study and was tested using the TLS scans collected from the six study plots (Figure 1). TLS scans in each plot were registered to the center scan (scan 1) to minimize error propagation, except the scan 4 in plot 2 and 6. The scan 4 in plot 2 was a tilted scan, which was registered to its corresponding horizontal scan (scan 3) to evaluate the performance of the proposed algorithm on registering tilted and horizontal scans. The scan 4 in plot 6 was registered to scan 3 because the distance between scan 4 and scan 1 was too large, and there were insufficient overlapped areas between them to ensure the success of registration

(Figure 1). The manual registration method was used to register the TLS scans as well following the same registration configuration. The installed high-reflectance registration targets were visually identified and used as tie points to coarsely register TLS scan pairs, and then the same fine registration procedure based on the ICP algorithm was used to achieve the final manual registration results. The manual registration process was performed in the RIEGL RiScan Pro software. These manual egistration results were used as references to evaluate the performance of the proposed method.

Two accuracy assessment parameters were calculated from the registration results of the proposed and manual methods, i.e., the standard deviation of registration errors provided by the ICP algorithm and the average distance residual calculated from the high-reflectance registration targets. The standard deviation of registration errors provided by the ICP algorithm was calculated as the standard deviation of distances from registered target TLS points to their closest source TLS points. It can provide an accuracy assessment value for each pair of registered TLS scans, but is reported that may underestimate the registration error because the closet source TLS points to target TLS points may be not true matches (Gressin et al., 2013). To address this issue, we further used the installed high-reflectance registration targets to calculate the average distance residual for each study plot, which was the average offset between the center of the same registration target from different TLS scans.

## 3. Results

Parameters in the proposed marker-free registration method are listed in Table 2. All parameters, except $\Delta h$ and $D_r$, had the same settings to register all TLS scan pairs. The height adjustment for slicing vertical layers ($\Delta h$), was set by visually determining whether the sliced vertical layers contained most trunks, and $D_r$ was determined by the distance between each pair of TLS scans (Table 3). The procedures of data redundancy reduction, vertical coarse registration, visual occlusion point extraction, horizontal coarse registration, and fine registration were conducted following the abovementioned steps.

**Table 2** List of parameters used in the proposed marker-free method for registering multi-scan TLS data in forest environments.

| Parameter | Description | Value |
|---|---|---|
| $\Delta h$ | The height adjustment for slicing vertical layer(s) | Table 3 |
| $D_r$ | The distance threshold for extracting visual occlusion point | Table 3 |
| $D_c$ | The distance threshold for data redundancy reduction | 30 m |
| $\Delta Z$ | The thickness of the vertical sliced layer(s) | 0.2 m |
| $I_A$ | The angular resolution for creating the angular grid | 0.1° |
| $I_D$ | The distance resolution for creating the angular grid | 0.1 m |
| $D_t$ | The pre-defined match distance threshold for compensating the potential offset between a visual occlusion point pair | 0.2 m |
| $D_e$ | The distance to create the buffer behind a visual occlusion point candidate for excluding false detections | 0.5 m |
| Voxel size | The size of voxels for determining ground points from TLS data | 0.5 m |

**Table 3** Distance between each pair of TLS scans, and the corresponding parameter setup for determining the height adjustment for slicing vertical layer(s) ($\Delta h$) and the distance threshold for extracting visual occlusion point ($D_r$).

| Plot | Registering scans | Distance between scans (m) | $\Delta h$ (m) | $D_r$ (m) |
|---|---|---|---|---|
| 1 | Scan 2 to 1 | 21.6 | 0 | 20 |
| | Scan 3 to 1 | 20.9 | 0 | 20 |

| | | | | |
|---|---|---|---|---|
| | Scan 4 to 1 | 21 | 0 | 20 |
| 2 | Scan 2 to 1 | 6.6 | 0 | 10 |
| | Scan 3 to 1 | 12.0 | 0 | 15 |
| | Scan 4 to 3 | 0.2 | 0 | 10 |
| 3 | Scan 2 to 1 | 9.3 | 0, 0.5 | 15 |
| | Scan 3 to 1 | 5.6 | 0, 0.5 | 10 |
| | Scan 4 to 1 | 9.4 | 0, 0.5 | 15 |
| 4 | Scan 2 to 1 | 0.4 | 0 | 10 |
| | Scan 3 to 1 | 13.8 | 0 | 15 |
| | Scan 4 to 1 | 16.0 | 0 | 15 |
| 5 | Scan 2 to 1 | 4.2 | 0.1 | 10 |
| | Scan 3 to 1 | 7.3 | 0.1 | 10 |
| 6 | Scan 2 to 1 | 6.8 | 0 | 10 |
| | Scan 3 to 1 | 7.1 | 0 | 10 |
| | Scan 4 to 3 | 6.5 | 0 | 10 |

As the key feature to register multi-scan TLS data, more than 17 visual occlusion points were detected in all source and target TLS data (Table 4). Plot 1 had the highest number of identified visual occlusion points among all plots. With the increase of canopy complexity, the number of identified visual occlusion points decreased significantly (Table 1 and 4). For the same scan, the number of identified visual occlusion points decreased with $D_r$ (Table 3 and 4). The number of matched visual occlusion points identified from the enumeration process was larger than 4 at all pairs of registering TLS scans (Table 4), and decreased with the increasing complexity of forest canopy as well (Table 1 and 4).

**Table 4** The number of visual occlusion points identified from the source TLS scan ($P_s$) and the target TLS scan ($P_t$), the number of matched visual occlusion points identified from the enumeration process ($P_s \cap P_t$), and the standard deviation of registration errors provided by the ICP function of the RIEGL RiScan Pro software.

| Plot | Registering scans | $P_s$ | $P_t$ | $P_s \cap P_t$ | Standard deviation (cm) | |
|---|---|---|---|---|---|---|
| | | | | | Proposed method | Manual method |
| 1 | Scan 2 to 1 | 72 | 72 | 21 | 0.3 | 0.2 |
| | Scan 3 to 1 | 72 | 58 | 16 | 0.5 | 0.5 |
| | Scan 4 to 1 | 72 | 52 | 16 | 0.2 | 0.3 |
| 2 | Scan 2 to 1 | 24 | 23 | 5 | 0.6 | 0.6 |
| | Scan 3 to 1 | 40 | 27 | 6 | 0.4 | 0.5 |
| | Scan 4 to 3 | 19 | 17 | 5 | 0.3 | 0.3 |
| 3 | Scan 2 to 1 | 26 | 24 | 5 | 0.8 | 0.6 |
| | Scan 3 to 1 | 21 | 24 | 6 | 0.7 | 0.5 |
| | Scan 4 to 1 | 26 | 20 | 4 | 0.7 | 0.5 |
| 4 | Scan 2 to 1 | 21 | 25 | 4 | 0.3 | 0.3 |
| | Scan 3 to 1 | 36 | 19 | 6 | 0.9 | 0.7 |
| | Scan 4 to 1 | 36 | 17 | 6 | 0.8 | 0.9 |
| 5 | Scan 2 to 1 | 30 | 26 | 13 | 0.1 | 0.2 |
| | Scan 3 to 1 | 30 | 34 | 10 | 0.3 | 0.2 |
| 6 | Scan 2 to 1 | 32 | 27 | 6 | 0.2 | 0.3 |
| | Scan 3 to 1 | 32 | 30 | 5 | 0.3 | 0.3 |
| | Scan 4 to 3 | 30 | 26 | 5 | 0.5 | 0.4 |

The final fine registration results are shown in Figure 8. As can be seen, all TLS scans were aligned properly. From the profile and enlarged segment examples, we can see that the registered TLS data described the structure characteristics more completely since they depicted the forest canopy from different viewing angles (Figure 8b and c). The standard deviations of registration errors provided by the ICP function were lower than 1 cm in all study plots. A higher number of matched visual occlusion points did not ensure a higher registration accuracy. The lowest standard deviations happened between scan 2 and scan 1 in plot 5, and it had 13 pairs of matched visual occlusion points, which was lower than the number of pairs in plot 1 (Table 4). The accuracy evaluated by the high-reflectance registration targets was lower than that provided by the ICP algorithm. The average distance residual ranged from 2.4 - 6.8 cm in the six study plots, and plot 3 had the largest average distance residual (Table 5). The manual registration method had similar registration accuracies as the proposed method. The differences of both accuracy measures between the proposed method and the manual registration method were smaller than 0.6 cm (Table 4 and Table 5).

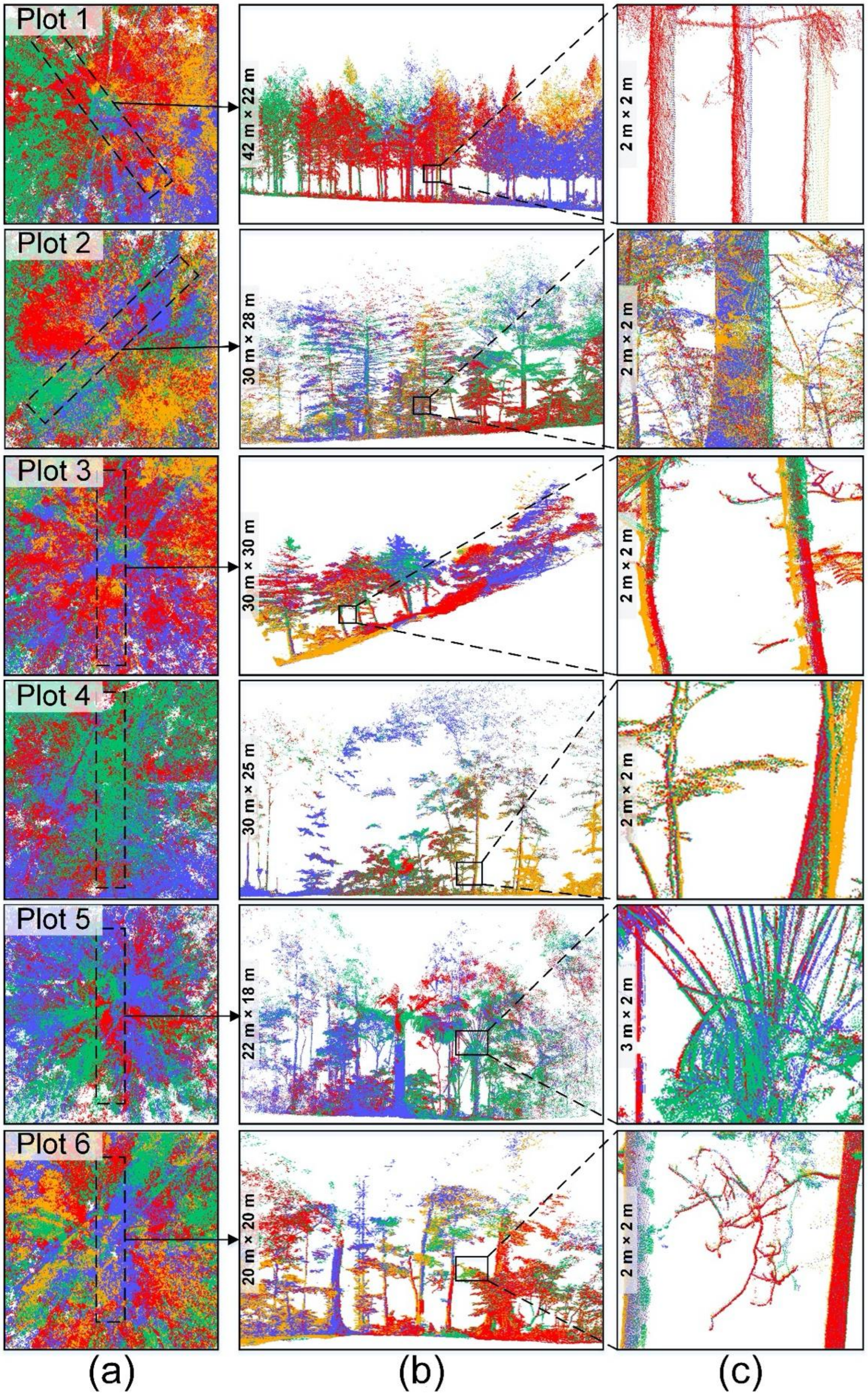


**Figure 8** (a) The registered TLS data in all six plots using the proposed marker-free method; (b)

point cloud profile examples in each plot, and (c) enlarged point cloud segments in the profiles. Note that point color from each scan position is in correspondence with the color of the scan in Figure 1c, and the numbers presented on the left short side of (b) and (c) are the size of the profiles or segments.

**Table 5** Average distance residuals of the registration results using the proposed method and the manual registration method in each plot.

| Plot | Proposed method (cm) | Manual method (cm) |
|---|---|---|
| 1 | 2.5 | 2.7 |
| 2 | 2.4 | 2.3 |
| 3 | 6.8 | 6.6 |
| 4 | 4.6 | 4.7 |
| 5 | 4.3 | 4.5 |
| 6 | 4.6 | 4.0 |
| Mean | 4.2 | 4.1 |

# 4. Discussion

## 4.1 Overall performance of the proposed marker-free registration method

TLS technology has been recognized as an efficient and accurate tool for quantifying forest structure parameters (Watt and Donoghue, 2005; Newnham et al., 2015) but registering multi-scan TLS data has been a tedious and time-consuming task that limits its application in large-scale forestry studies (Liang et al., 2014). In this study, we proposed a marker-free method that can automatically register multi-scan TLS data. Overall, the proposed algorithm performed well in all 6 plots with different vegetation characteristics. The registration accuracy was equivalent to the manual registration results using high-reflectance registration targets, and the slight difference between these two methods might be cuased by random errors of the TLS scanner the ICP algorithm. The efficiency of the registration process has been much improved. It took less than 10 mins to register two TLS scans without the ICP fine registration step using the proposed methods in all six plots. For comparison, it usually took an experienced operator 0.5 hr to 2 hrs to manually register two TLS scans without the ICP fine registration step.

Compared with other marker-free point cloud registration algorithms, the proposed algorithm has the advantages of being independent from individual tree attributes (e.g., tree location, tree height, tree stem maps), which are often estimated through complex and time-consuming post-processing steps, such as ground point filtering, normalization, individual tree segmentation (Othmani et al., 2013; Kelbe et al., 2016; Liu et al., 2017; Giannetti et al., 2018; Guan et al., 2019; Polewski et al., 2019). This may make the efficiency of these algorithms even lower than the manual registration method. Moreover, the accuracy of individual tree segmentation and tree attribute extraction might be low in the forests of dense canopy and high plant diversity (e.g., rainforest with dense undercanoy vegetation) (Jing et al., 2012; Yang et al., 2019), and errors in the extracted individual tree attributes might cause failures to these algorithms (Guan et al., 2019). The proposed algorithm uses shaded areas that naturally existed in raw TLS data as the estimates of tree trunk locations since laser pulses cannot penetrate tree trunks and should leave blank areas behind tree trunks. Therefore, it does not need to process TLS raw data to extract individual tree attributes, which can improve both the efficiency and robustness of multi-scan TLS data registration.

## 4.2 Factors influencing the performance of the proposed method

The success of horizontal registration is the essential precondition for the proposed method and the success rate of horizontal registration is determined by the number of matched visual occlusion points. If the number of matched visual occlusion points is too small, the horizontal registration may fail. As can be seen from Table 3 and Table 4, the number of matched visual occlusion points is influenced by the complexity of understory vegetation and the distance between registering scans. In an area with tall and dense understory vegetation, laser pulses can be significantly blocked by the understory vegetation, and shaded areas caused by tree trunks might become less observable. Therefore, the likelihood of finding enough matched visual occlusion points in the overlapped areas between two adjacent scans becomes much lower. To resolve this issue, it is recommended to increase $\Delta h$ to slice vertical layer(s) higher than understory vegetation, so that enough visual occlusion points can be identified in the overlapped areas between two scans. In this study, we found that increased distance between registering scans can reduce the change to recognize enough visual occlusion points for registration. Therefore, we recommend that the distance between the two scans should be less than 15 m to increase the success rate of coarse registration. With sufficient matched visual occlusion points to ensure the success of coarse registration, the final registration accuracy of the proposed algorithm purely depends on the ICP algorithm.

### 4.3 Parameter sensitivity analysis

The robustness of the proposed method can be seen in the high registration accuracy over all six plots with different vegetation characteristics. There are a total of nine parameters in the proposed method (Table 2). A discussion of how each parameter is determined and the sensitivity of the proposed method to each parameter is presented here.

In this study, the same parameter settings for $\Delta Z$, $I_A$, $I_D$, $D_t$, $D_e$ and voxel size were used for the registration practices of all 17 TLS scans. Parameter $\Delta Z$ is used to control the thickness of the sliced vertical layer (Figure 4). In previous studies, the sliced vertical layer has been widely used to automatically extract DBH with a thickness ranging from 0.05 m to 0.5 m (Olofsson et al., 2014; Stovall et al., 2017; Liu et al., 2018). $I_A$ and $I_D$ are the angular and distance resolutions for creating the angular grid (Figure 5), and $I_A$ are used as the rotation interval in the enumeration process to match visual occlusion points as well. Therefore, they should be set to relatively small values to ensure higher accuracy ($I_A$=0.1$^{\circ}$ and $I_D$=0.1 m in this study). Parameter $D_t$ is the distance for compensating the potential offset between a visual occlusion point pair. Since this offset cannot be larger than the DBH of trees, $D_t$ can be set around the average DBH of the study area. Therefore, a value of 0.2 m could be reasonable for $D_t$. Parameter $D_e$ is the distance behind an identified visual occlusion point to create the buffer for examining the correctness of the identification result (Figure 5). It is designed to compensate for the scenario of inclined trees, which may leave tree trunk point behind the a visual occlusion point. Assuming a tree with a large inclination angle of 60°, the maximum distance behind the tree to the visual occlusion point could be 0.4 m when $\Delta Z$ was set as 0.2 m. Therefore, a value of 0.5 m should be a safe choice for $D_e$. The voxel size for determining ground points can be set to 0.5 m, which is a commonly suggested value for deriving forest stand attributes from TLS data in the literature (Popescu and Zhao, 2008; Wu et al., 2013). It should be noted that the voxel-based process does not aim to identify true ground points. Instead, it aims to identify points near the ground surface (may include low vegetation points as well) to perform the vertical coarse registration. Therefore, it is not a crucial parameter for the proposed method.

To further evaluate the sensitivity of the proposed algorithm to $\Delta Z$, $I_A$, $I_D$, $D_t$, $D_e$ and voxel size, we run the proposed coarse registration procedure repetitively by altering one parameter with a constant interval while keeping other parameters as the default settings (Table 2). Scan 1 and 2 in plot 1 were used as an example to perform the sensitivity analysis. As can be seen in Figure 9, the number of matched visual occlusion points fluctuated around 20 with variations of $D_e$ and voxel size, indicating the proposed algorithm is insensitive to these parameters. Moreover, the number of matched visual occlusion points increased with $\Delta Z$ and $D_t$, while decreased with $I_A$ and $I_D$. Nevertheless, a sufficient number of matched visual occlusion points could still be identified even with the most extreme circumstances (except when $I_D$ > 0.9 m). These results indicated that the proposed method is robust to the settings of $\Delta Z$, $I_A$, $I_D$, $D_t$, $D_e$ and voxel size. Following the abovementioned guidance for setting these parameters, a universal parameter set of these six parameters could be possibly achieved for most TLS registration applications in forest environments.

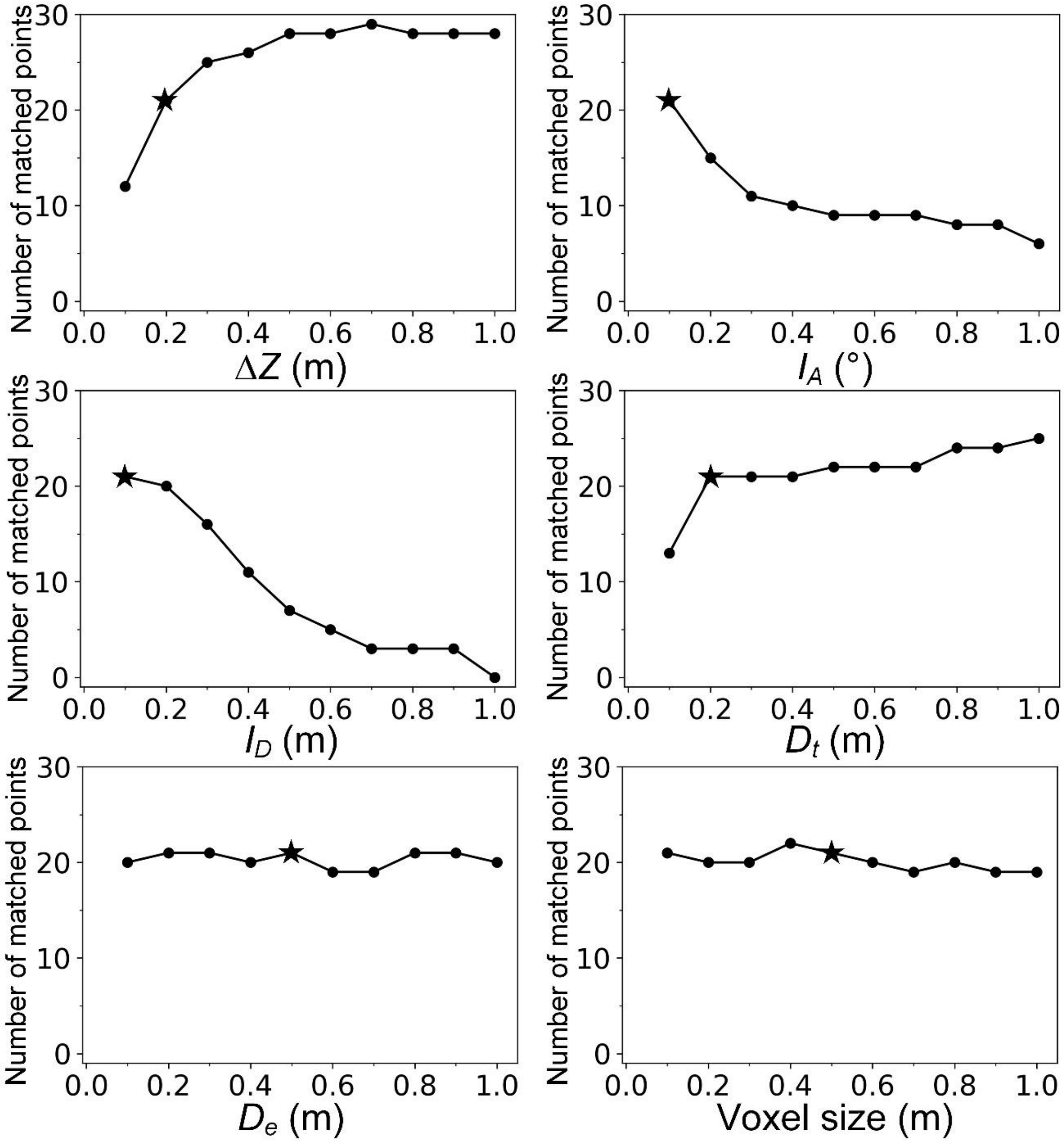


**Figure 9** The sensitivity of the proposed method to the setting of $\Delta Z,\ I_A,\ I_D\ D_t,\ D_e$ and voxel size. Here, the experiment was conducted using the scan pair of scan 1 and 2 in plot 1. Each run only altered one parameter setting. The registration results are represented by the number of matched points. The higher the number is, the higher the success rate of coarse registration is. Black pentagram represents the used parameter values in this study (Table 2).

Parameter $\Delta h$ is used to adjust the base height for slicing vertical layer(s). As shown in Figure 4, the default base height for slicing vertical layer(s) should be set to the height of the TLS scanner. The TLS scanner is usually set to a height with good visibility to the surrounding trees, therefore, the default value for $\Delta h$ is zero. However, if the TLS scanner is surrounded by tall and dense vegetation, the visibility of the TLS scanner can be significantly reduced. Therefore, we recommend using a simple trial-and-error method to increase $\Delta h$ with an interval of 0.1 m to ensure we can see as many tree trunks as possible in the sliced vertical layer. A visual examination can be used to determine whether the selected value for $\Delta h$ is appropriate after each try. In a sloped terrain, the horizontally sliced vertical layer can be intercepted by the ground surface, and therefore the visibility at a single sliced layer might be reduced (Figure 4). To solve this issue, we recommend using a strategy similar to the experiment in plot 5, which sliced multiple height layers at different base heights. The same trial-and-error method can be used to determine the value of $\Delta h$ of other layers. It is recommended to only slice one vertical layer if it is enough for the coarse registration procedure because multiple vertical layers may introduce more errors in identifying visual occlusion points.

Parameter $D_c$ is the distance threshold from the scan center to reduce data redundancy, which is designed to improve the registration efficiency (Figure 5). This value can be determined by visually examining the original TLS data following the principle of removing sparse points on the edge of a scan. Parameter $D_r$, a distance threshold smaller than $D_c$, is designed to further reduce the extent of the study area so that the visual occlusion point filtering procedure based on a user-defined buffer can be performed (Figure 5). $D_r$ can also influence the registration efficiency. The larger the $D_r$ is, the more potential visual occlusion points can be found, and the time consumption of the enumeration process increases drastically as well. Using a laptop with an Intel Core i5-6300HQ CPU @ 2.30 GHz CPU, 4 GB of RAM, it took around 20 seconds for registering scans with around 20 identified visual occlusion points (e.g., scan 4 and 3 in plot 2), and around 5 mins for registering scans with around 40 identified visual occlusion points (e.g., scan 3 and scan 1 in plot 2). Therefore, $D_r$ is an important parameter for balancing processing speed and success rate. To further evaluate the influence of $D_r$ on the registration success rate, we simulated a source scan from the registered point cloud of all scans in plot 1 and simulated target scans with a distance to the simulated source scan increasing from 5 m to 20 m at intervals of 5 m. Given a scan position, a high-resolution angular gird was created from the registered point cloud of all scans in plot 1, and points in the innermost pixels were extracted as the simulated scan. For each scan distance combination, $D_r$ was changed from 5 m to 25 m at intervals of 5 m, and a total of 20 registration instances were run (Table 6). In general, the number of extracted visual occlusion points increased with $D_r$ and decreased with the scan distance under all registration combinations, as well as the number of matched visual occlusion points. When $D_r$ was set to smaller than the scan distance, the corresponding coarse registration failed since an insufficient number of matched visual occlusion points was found (Table 6). Therefore, we recommend setting $D_r$ slightly larger than the scan distance to ensure the high success rate. One exception for this recommendation is the registration practice between tilted and horizontal scans at the same location. As can be seen in Table 5, a sufficient number of matched visual occlusion points could be detected when the scan distance was 5 m and $D_r$ was set as 10 m. Therefore, it would be safe to recommend using a $D_r$ around 10 m for practices of registering tilted and horizontal scans.

**Table 5** Visual occlusion point extraction results from registration instances with different scan distance ($d$) and $D_r$.

| $D_r$ (m) | $P_s$ | $d$=5 m | | $d$=10 m | | $d$=15 m | | $d$=20 m | |
|---|---|---|---|---|---|---|---|---|---|
| | | $P_t$ | $P_s \cap P_t$ | $P_t$ | $P_s \cap P_t$ | $P_t$ | $P_s \cap P_t$ | $P_t$ | $P_s \cap P_t$ |
| 5 | 9 | 6 | 5 | 5 | 0 | 4 | 0 | 4 | 0 |
| 10 | 21 | 19 | 14 | 18 | 7 | 13 | 0 | 17 | 0 |
| 15 | 44 | 33 | 26 | 37 | 18 | 26 | 6 | 33 | 4 |
| 20 | 64 | 57 | 42 | 50 | 28 | 45 | 15 | 54 | 10 |
| 25 | 88 | 80 | 54 | 74 | 45 | 66 | 27 | 77 | 25 |

The success of the proposed method relies on the correct detection of visual occlusion points, and misinterpreted visual occlusion points may cause the coarse registration step to fail. Misidentified visual occlusion points are prone to occur in complex forests. To further discuss the sensitivity of the proposed method to errors in the visual occlusion point detection results, we run the visual occlusion point matching procedure by gradually adding extra false visual occlusion points or removing true visual occlusion points (Figure 10). The process was based on the two simulated scans in Table 5 with a scan distance of 10 m and a $D_r$ of 10 m, because the scan distance of 10 m was recommended by many previous studies to collect TLS data in forest environments (Wilkes et al., 2017; Ma et al., 2018; Pyörälä et al., 2019). The proposed algorithm succeeded in most scenarios (Figure 10), even when the omission error (i.e., removing true visual occlusion points) or commission error (i.e., adding false visual occlusion points) were around 67% because most of them might not happen in the overlapped areas between two scans. However, when the number of matched visual occlusion points was lower than 3, the success rate of registration was reduced significantly because of higher omission and commission error may cause higher chances of false matches.

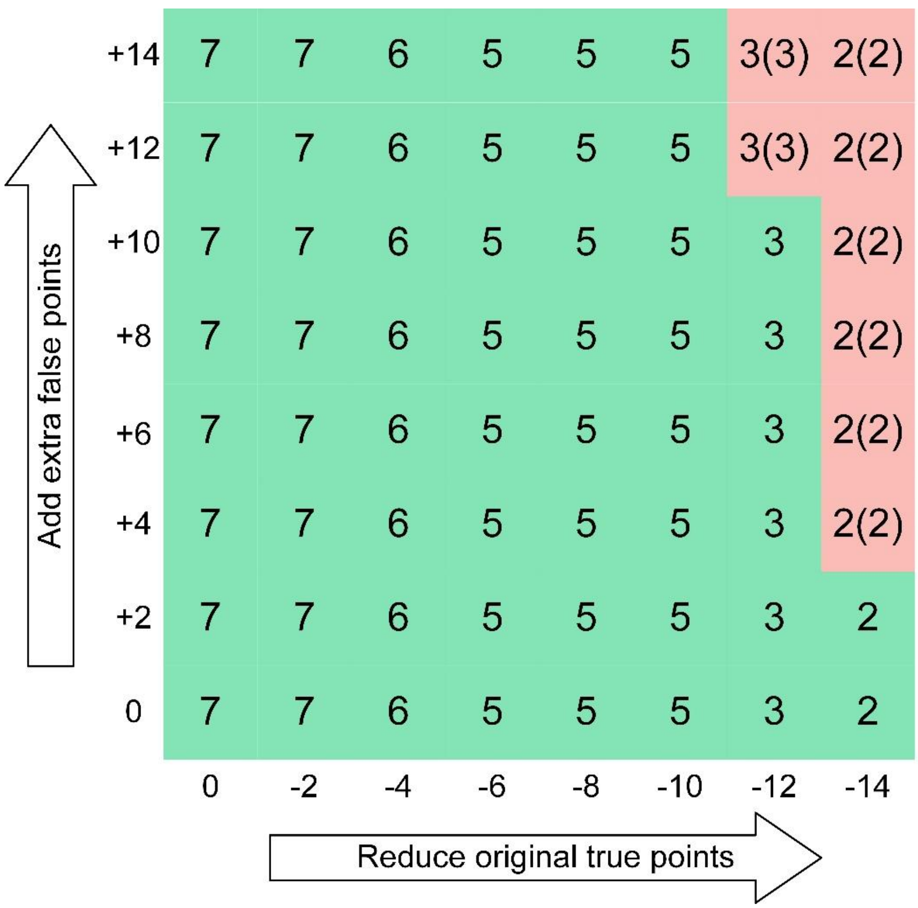


**Figure 10** The sensitivity of the proposed method to errors in the identified visual occlusion points. Numbers in the squares represent the number of matched visual occlusion points, while numbers in the parenthesis represent the number of falsely matched visual occlusion points; green squares represent the corresponding registration runs are succeeded, and red squares

represent the corresponding registration runs are failed; and "-" and "+" represent reducing original true visual occlusion points or adding false visual occlusion points. All runs were performed based on the two simulated scans in Table 5 with a scan distance of 10 m and a $D_r$ of 10 m.

In brief, the proposed method shows strong robustness under different parameter settings. The default values used for six of the nine parameters (i.e., $\Delta Z$, $I_A$, $I_D$, $D_t$, $D_e$ and voxel size) are applicable to most TLS registration applications in forests, and the remaining three parameters (i.e., $\Delta h$, $D_c$, $D_r$ ) can be easily determined from the TLS scanner setup, forest conditions or a trial-and-error process. Moreover, the proposed method has a strong tolerance to errors in the visual occlusion point detection results.

### 4.4 Limitations of the current study

The major contribution of this study is that it provides a novel marker-free method for automatically registering multi-scan TLS data, and has a high registration accuracy while maintaining robustness under complex forest conditions. Nevertheless, there are still limitations. First, with the increase of identified visual occlusion points, the computation time of the enumeration process increased exponentially. In the future, parallel processing and graphical processing unit acceleration techniques (Li et al., 2018) could be integrated into the enumeration process to further improve the efficiency. Second, the proposed method used sliced layers without normalizing the raw point cloud to extract visual occlusion points. Although a vertical adjustment procedure was used, the sliced layers from different TLS scans might still be at different height strata. Future studies are still needed on how to eliminate the height differences between sliced layers from different TLS scans. Third, current ICP algorithms used for fine registration were designed for point data collected in environments with rich geometric features (e.g., indoor and urban environments) (Von Hansen et al., 2008; Wu et al., 2014, He et al., 2017), which fail frequently in forest environments. This is especially true when the point density in overlapped areas is relatively low (Theiler et al., 2015). Moreover, current ICP algorithms tend to give higher weights to areas with higher point density (Järemo Lawin et al., 2018), which is commonly seen in the TLS data in forests. This may result in larger errors in areas with low point density in the final registration process. A new ICP algorithm considering the characteristics of TLS data in forest environments (e.g., uneven point density distribution, lacking geometric features) needs to be developed.

## 5. Conclusions

This study proposed a novel marker-free method for registering multi-scan TLS data. Its main principle is to use shaded areas as the key feature to match TLS scans. The proposed method was tested with 17 pairs of TLS scans collected in 6 plots across China, ranging in vegetation types from planted conifer forest to rainforest. Results showed that the proposed method successfully identified enough matched visual occlusion points for coarse registration under complex forest environments and scan setups. The final registration errors of the proposed method in all 17 pairs of TLS scans were equivalent to those of the manual registration method. The registration efficiency was improved significantly because it eliminated the process of setting up hand-crafted registration targets in the field and visually identifying registration targets in the collected TLS data for coarse registration. Moreover, the proposed method can keep a success rate with the change of parameter settings, and all parameters can be either obtained by the TLS scan setup (e.g., scanner height, distance between scans) and forest conditions (e.g., terrain slope, understory vegetation height) or by a simple trial-and-error process. We believe that the proposed method has great potential to reduce the time and cost of collecting TLS data in forests, and therefore expand the application of the TLS technique in large-scale forest managements and studies.

## Acknowledgements

This work was supported by the Frontier Science Key Programs of the Chinese Academy of Sciences (QYZDY-SSW-SMC011), National Natural Science Foundation of China (41871332), and the CAS Pioneer Hundred Talents Program. The source code and the command-line based tool of the proposed method will be available at http:// www.3decology.org/.

## References

Gressin A, Mallet C, Demantké J, David N. Towards.,2013. 3D lidar point cloud registration improvement using optimal neighborhood knowledge. ISPRS Journal of Photogrammetry and Remote Sensing 79, 240-251.

Basantes, J., Padilla-Almeida, O., Toulkeridis, T., Ordoñez, E., Zapata-Vela, J., Zapata-Vela, A.C., Rojas, S., 2019. Dasometric Analysis Applying Terrestrial Laser Scanner and Conventional Techniques for the Estimation of Aboveground Biomass in a Forest of the Inter-Andean Valley in Ecuador, in: 2019 Sixth International Conference on EDemocracy & EGovernment (ICEDEG). IEEE, 334–337.

Bauwens, S., Bartholomeus, H., Calders, K., Lejeune, P., 2016. Forest inventory with terrestrial LiDAR: A comparison of static and hand-held mobile laser scanning. Forests 7, 127.

Brolly, G., Király, G., 2009. Algorithms for stem mapping by means of terrestrial laser scanning. Acta Silvatica et Lignaria Hungarica 5, 119–130.

Cabo, C., Ordóñez, C., López-Sánchez, C.A., Armesto, J., 2018. Automatic dendrometry: Tree detection, tree height and diameter estimation using terrestrial laser scanning. International journal of applied earth observation and geoinformation 69, 164–174.

Che, E., Olsen, M.J., 2017. Fast ground filtering for TLS data via Scanline Density Analysis. ISPRS Journal of Photogrammetry and Remote Sensing 129, 226–240.

Comaniciu, D., Meer, P., 2002. Mean shift: A robust approach toward feature space analysis. IEEE Transactions on Pattern Analysis & Machine Intelligence 603–619.

Dassot, M., Constant, T., Fournier, M., 2011. The use of terrestrial LiDAR technology in forest science: application fields, benefits and challenges. Annals of forest science 68, 959–974.

Giannetti, F., Puletti, N., Quatrini, V., Travaglini, D., Bottalico, F., Corona, P., Chirici, G., 2018. Integrating terrestrial and airborne laser scanning for the assessment of single-tree attributes in Mediterranean forest stands. European Journal of Remote Sensing 51, 795–807.

Guan, H., Su, Y., Hu, T., Wang, R., Yang, Q., Sun, X., Li, Y., Jin, S., Zhang, J., Ma, Q., Liu, M., Wu, F., Guo, Q., 2019. A Novel Framework to Automatically Fuse Multiplatform LiDAR Data in Forest Environments Based on Tree Locations. IEEE Transactions on Geoscience and Remote Sensing 1–13.

He, Y., Liang, B., Yang, J., Li, S., He, J., 2017. An iterative closest points algorithm for registration of 3D laser scanner point clouds with geometric features. Sensors 17, 1862.

Heinzel, J., Huber, M.O., 2017. Detecting tree stems from volumetric TLS data in forest environments with rich understory. Remote Sensing 9, 9.

Henning, J.G., Radtke, P.J., 2008. . ISPRS Journal of Photogrammetry and Remote Sensing 63, 68–83.

Henning, J.G., Radtke, P.J., 2006. Detailed stem measurements of standing trees from ground-based scanning lidar. Forest Science 52, 67–80.

Hilker, T., Coops, N.C., Culvenor, D.S., Newnham, G., Wulder, M.A., Bater, C.W., Siggins, A., 2012. A simple technique for co-registration of terrestrial LiDAR observations for forestry applications. Remote sensing letters 3, 239–247.

Järemo Lawin, F., Danelljan, M., Shahbaz Khan, F., Forssén, P.-E., Felsberg, M., 2018. Density adaptive point set registration, in: Proceedings of the IEEE Conference on Computer

Vision and Pattern Recognition. 3829–3837.

Jing, L., Hu, B., Li, J., Noland, T., 2012. Automated delineation of individual tree crowns from LiDAR data by multi-scale analysis and segmentation. Photogrammetric Engineering & Remote Sensing 78, 1275–1284.

Kelbe, D., Van Aardt, J., Romanczyk, P., Van Leeuwen, M., Cawse-Nicholson, K., 2016. Marker-free registration of forest terrestrial laser scanner data pairs with embedded confidence metrics. IEEE Transactions on Geoscience and Remote Sensing 54, 4314–4330.

Li, W., Guo, Q., Tao, S., Su, Y., 2018. VBRT: A novel voxel-based radiative transfer model for heterogeneous three-dimensional forest scenes. Remote sensing of environment 206, 318–335.

Li, Y., Guo, Q., Su, Y., Tao, S., Zhao, K., Xu, G., 2017. Retrieving the gap fraction, element clumping index, and leaf area index of individual trees using single-scan data from a terrestrial laser scanner. ISPRS Journal of Photogrammetry and Remote Sensing 130, 308–316.

Liang, X., Hyyppä, J., Kaartinen, H., Lehtomäki, M., Pyörälä, J., Pfeifer, N., Holopainen, M., Brolly, G., Francesco, P., Hackenberg, J., others, 2018. International benchmarking of terrestrial laser scanning approaches for forest inventories. ISPRS journal of photogrammetry and remote sensing 144, 137–179.

Liang, X., Hyyppä, J., Kukko, A., Kaartinen, H., Jaakkola, A., Yu, X., 2014. The use of a mobile laser scanning system for mapping large forest plots. IEEE Geoscience and Remote Sensing Letters 11, 1504–1508.

Liang, X., Kankare, V., Hyyppä, J., Wang, Y., Kukko, A., Haggrén, H., Yu, X., Kaartinen, H., Jaakkola, A., Guan, F., others, 2016. Terrestrial laser scanning in forest inventories. ISPRS Journal of Photogrammetry and Remote Sensing 115, 63–77.

Lin, Y., Holopainen, M., Kankare, V., Hyyppä, J., 2014. Validation of mobile laser scanning for understory tree characterization in urban forest. IEEE Journal of Selected Topics in Applied Earth Observations and Remote Sensing 7, 3167–3173.

Lin, Y., Hyyppä, J., Jaakkola, A., Yu, X., 2012. Three-level frame and RD-schematic algorithm for automatic detection of individual trees from MLS point clouds. International journal of remote sensing 33, 1701–1716.

Liu, G., Wang, J., Dong, P., Chen, Y., Liu, Z., 2018. Estimating Individual Tree Height and Diameter at Breast Height (DBH) from Terrestrial Laser Scanning (TLS) Data at Plot Level. Forests 9, 398.

Liu, J., Liang, X., Hyyppä, J., Yu, X., Lehtomäki, M., Pyörälä, J., Zhu, L., Wang, Y., Chen, R., 2017. Automated matching of multiple terrestrial laser scans for stem mapping without the use of artificial references. International journal of applied earth observation and geoinformation 56, 13–23.

Ma, L., Zheng, G., Wang, X., Li, S., Lin, Y., Ju, W., 2018. Retrieving forest canopy clumping index using terrestrial laser scanning data. Remote sensing of environment 210, 452–472.

Miliaresis, G., Kokkas, N., 2007. Segmentation and object-based classification for the extraction of the building class from LIDAR DEMs. Computers & Geosciences 33, 1076–1087.

Newnham, G.J., Armston, J.D., Calders, K., Disney, M.I., Lovell, J.L., Schaaf, C.B., Strahler, A.H., Danson, F.M., 2015. Terrestrial laser scanning for plot-scale forest measurement. Current Forestry Reports 1, 239–251.

Olofsson, K., Holmgren, J., Olsson, H., 2014. Tree stem and height measurements using terrestrial laser scanning and the RANSAC algorithm. Remote sensing 6, 4323–4344.

Olsoy, P.J., Mitchell, J.J., Levia, D.F., Clark, P.E., Glenn, N.F., 2016. Estimation of big sagebrush leaf area index with terrestrial laser scanning. Ecological indicators 61, 815–821.

Othmani, A., Voon, L.F.L.Y., Stolz, C., Piboule, A., 2013. Single tree species classification from terrestrial laser scanning data for forest inventory. Pattern Recognition Letters 34, 2144–2150.

Panagiotidis, D., Surovỳ, P., Kuželka, K., 2016. Accuracy of Structure from Motion models in comparison with terrestrial laser scanner for the analysis of DBH and height influence on error behaviour. Journal of Forest Science 62, 357–365.

Pirotti, F., Guarnieri, A., Vettore, A., 2013. Ground filtering and vegetation mapping using multi-return terrestrial laser scanning. ISPRS Journal of Photogrammetry and Remote Sensing 76, 56–63.

Polewski, P., Yao, W., Cao, L., Gao, S., 2019. Marker-free coregistration of UAV and backpack LiDAR point clouds in forested areas. ISPRS journal of photogrammetry and remote sensing 147, 307–318.

Popescu, S.C., Zhao, K., 2008. A voxel-based lidar method for estimating crown base height for deciduous and pine trees. Remote sensing of environment 112, 767–781.

Puttonen, E., Lehtomäki, M., Litkey, P., Näsi, R., Feng, Z., Liang, X., Wittke, S., Pandžić, M., Hakala, T., Karjalainen, M., others, 2019. A Clustering Framework for Monitoring Circadian Rhythm in Structural Dynamics in Plants From Terrestrial Laser Scanning Time Series. Frontiers in plant science 10, 486.

Pyörälä, J., Saarinen, N., Kankare, V., Coops, N.C., Liang, X., Wang, Y., Holopainen, M., Hyyppä, J., Vastaranta, M., 2019. Variability of wood properties using airborne and terrestrial laser scanning. Remote Sensing of Environment 235, 111474.

Roşca, S., Suomalainen, J., Bartholomeus, H., Herold, M., 2018. Comparing terrestrial laser scanning and unmanned aerial vehicle structure from motion to assess top of canopy structure in tropical forests. Interface focus 8, 20170038.

Sigrist, P., Coppin, P., Hermy, M., 1999. Impact of forest canopy on quality and accuracy of GPS measurements. International Journal of Remote Sensing 20, 3595–3610.

Stovall, A.E., Vorster, A.G., Anderson, R.S., Evangelista, P.H., Shugart, H.H., 2017. Non-destructive aboveground biomass estimation of coniferous trees using terrestrial LiDAR. Remote sensing of environment 200, 31–42.

Theiler, P.W., Wegner, J.D., Schindler, K., 2015. Globally consistent registration of terrestrial laser scans via graph optimization. ISPRS journal of photogrammetry and remote sensing 109, 126–138.

Travelletti, J., Malet, J.-P., Samyn, K., Grandjean, G., Jaboyedoff, M., 2013. Control of landslide retrogression by discontinuities: evidence by the integration of airborne-and ground-based geophysical information. Landslides 10, 37–54.

Tremblay, J.-F., Béland, M., 2018. Towards operational marker-free registration of terrestrial lidar data in forests. ISPRS journal of photogrammetry and remote sensing 146, 430–435.

Trochta, J., Král, K., Janík, D., Adam, D., 2013. Arrangement of terrestrial laser scanner positions for area-wide stem mapping of natural forests. Canadian journal of forest research 43, 355–363.

Vaaja, M., Virtanen, J.-P., Kurkela, M., Lehtola, V., Hyyppä, J., Hyyppä, H., others, 2016. The effect of wind on tree stem parameter estimation using terrestrial laser scanning. ISPRS Ann. Photogramm., Remote Sens. Spatial Inf. Sci 8, 117–122.

Von Hansen, W., Gross, H., Thoennessen, U., 2008. Line-based registration of terrestrial and airborne LIDAR data. Int. Arch. Photogramm. Remote Sens. Spat. Inf. Sci 37, 161–166.

Wang, Z., Brenner, C., others, 2008. Point based registration of terrestrial laser data using intensity and geometry features. Int. Arch. Photogramm. Remote Sens. Spat. Inf. Sci 37, 583–590.

Watt, P., Donoghue, D., 2005. Measuring forest structure with terrestrial laser scanning. International Journal of Remote Sensing 26, 1437–1446.

Wilkes, P., Lau, A., Disney, M., Calders, K., Burt, A., de Tanago, J.G., Bartholomeus, H., Brede, B., Herold, M., 2017. Data acquisition considerations for terrestrial laser scanning of forest plots. Remote Sensing of Environment 196, 140–153.

Wu, B., Yu, B., Yue, W., Shu, S., Tan, W., Hu, C., Huang, Y., Wu, J., Liu, H., 2013. A voxel-based method for automated identification and morphological parameters estimation of individual street trees from mobile laser scanning data. Remote Sensing 5, 584–611.

Wu, H., Scaioni, M., Li, H., Li, N., Lu, M., Liu, C., 2014. Feature-constrained registration of building point clouds acquired by terrestrial and airborne laser scanners. Journal of Applied Remote Sensing 8, 083587.

Yang, Q., Su, Y., Jin, S., Kelly, M., Hu, T., Ma, Q., Li, Y., Song, S., Zhang, J., Xu, G., others, 2019. The Influence of Vegetation Characteristics on Individual Tree Segmentation Methods with Airborne LiDAR Data. Remote Sensing 11, 2880.

Zhao, X., Su, Y., Li, W., Hu, T., Liu, J. and Guo, Q., 2018. A comparison of LiDAR filtering algorithms in vegetated mountain areas. Canadian Journal of Remote Sensing 44, 287-298.

Zhu, X., Wang, T., Skidmore, A.K., Darvishzadeh, R., Niemann, K.O., Liu, J., 2017. Canopy leaf water content estimated using terrestrial LiDAR. Agricultural and forest meteorology 232, 152–162.

# Declaration of Interest Statement

The authors confirm that there is no conflict of interest.